ACSNANO
www.acsnano.org
ARTICLE

Electrospun FeS_2@Carbon Fiber Electrode as a High Energy Density Cathode for Rechargeable Lithium Batteries

Yujie Zhu,[†,‡] Xiulin Fan,[‡] Liumin Suo,[‡] Chao Luo,[‡] Tao Gao,[‡] and Chunsheng Wang*[,‡]

[†]School of Chemistry and Environment, Beihang University, Beijing 100191, People's Republic of China
[‡]Department of Chemical and Biomolecular Engineering, University of Maryland, College Park, Maryland 20742, United States

Supporting Information

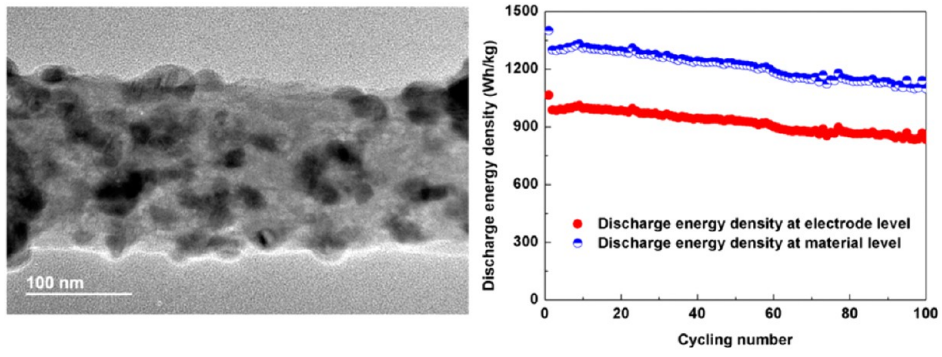

ABSTRACT: **In this study, an FeS_2@carbon fiber electrode is developed with FeS_2 nanoparticles either embedded in or attached to carbon fibers by using an electrospinning method. By applying this binder-free, metal-current-collector-free FeS_2@carbon fiber electrode, both the redox reaction and capacity decay mechanisms for the Li−FeS_2 system are revealed by changing the electrolyte (conventional carbonate electrolyte and a "solvent-in-salt"-type Li−S battery electrolyte) and working voltage ranges (1.0−3.0 V and 1.5−3.0 V *vs* Li/Li^+). The FeS_2@carbon fiber electrode shows stable cycling performance in both the conventional carbonate electrolyte and the solvent-in-salt-type Li−S battery electrolyte in the voltage range of 1.5−3.0 V. Electrochemical tests in the solvent-in-salt-type Li−S battery electrolyte indicate that the Li−FeS_2 system becomes a hybrid of the Li−S cell and Li−iron sulfide cell after the initial cycle. Based on the understanding on the capacity decay mechanisms, the cycling stability of the Li−FeS_2 system in the voltage range of 1.0−3.0 V is then significantly enhanced by coating the FeS_2@carbon fiber electrode with a thin layer of Al_2O_3. The Al_2O_3-coated electrode demonstrates excellent cycling performance with high discharge energy densities at both the material level (~1300 Wh/kg-FeS_2) and the electrode level (~1000 Wh/kg-FeS_2 electrode).**

KEYWORDS: *lithium-ion batteries, high energy density cathodes, FeS_2, electrospinning, atomic layer deposition*

The development of next generation high energy density lithium-ion (Li-ion) batteries is mainly restricted by the limited capacity provided by intercalation-type cathodes (*e.g.*, $LiCoO_2$, $LiFePO_4$, $LiMn_2O_4$), which possess a large portion of inert mass to accommodate the intercalation of Li-ions at the typical ratio of one Li-ion per transition metal. To circumvent this limit, much effort has been made to pursue cathode materials with higher capacities. Compounds, such as fluorides, sulfides, and oxides, *etc.*, that store Li-ions through the so-called conversion reactions can provide relatively higher capacities compared with intercalation-type cathodes because these materials can store more than one Li-ion per transition metal by fully utilizing all oxidation states of transition metals. Since the pioneering work of Poizot *et al.*,[1] conversion-reaction-based materials have been intensively studied. Recently, pyrite (cubic-FeS_2) has regained attention as a promising cathode material for rechargeable lithium batteries due to its high theoretical energy density (~1313 Wh/kg based on the reaction of $FeS_2 + 4Li = Fe + 2Li_2S$), low cost, earth abundance, and nontoxicity.[2−12] Compared with the popular Li−sulfur (Li−S) system at present, the Li−FeS_2 system is potentially safer because FeS_2 has a much higher melting point than sulfur. Also, considering the maturity of the Li−FeS_2 primary battery,[13] it would be much more viable to develop a

Received: November 9, 2015
Accepted: December 23, 2015
Published: December 23, 2015

DOI: 10.1021/acsnano.5b07081
ACS Nano 2016, 10, 1529−1538

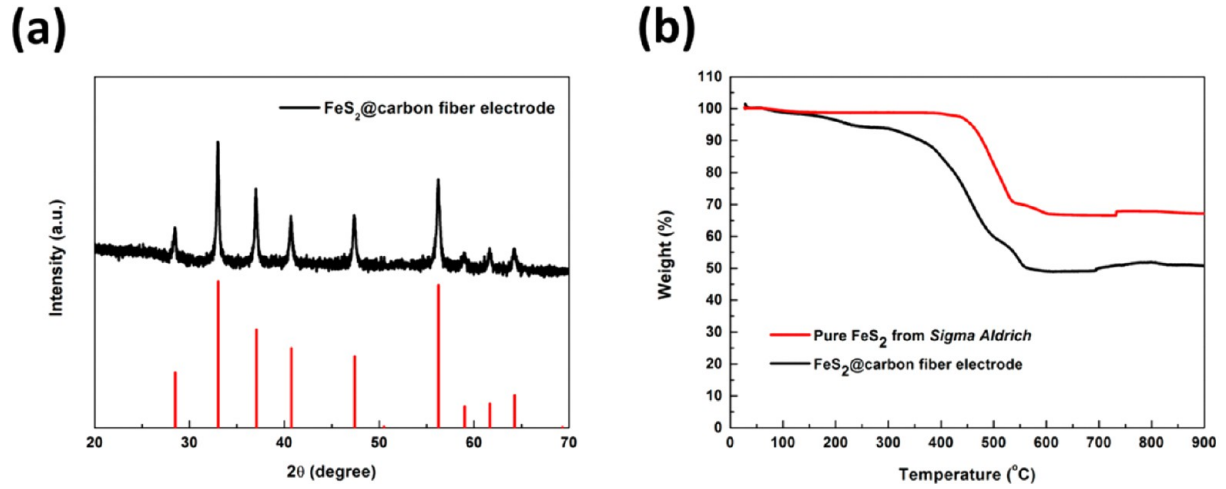

Figure 1. (a) Powder XRD pattern of FeS_2@carbon fiber electrode and (b) TGA results for commercial FeS_2 from Sigma-Aldrich and FeS_2@carbon fiber electrode.

commercial rechargeable Li−FeS_2 battery compared with Li−S battery, which is still in its very early stages.[14,15] However, the poor electrochemical reversibility of Li−FeS_2 chemistry has severely handicapped the utilization of FeS_2 in rechargeable lithium batteries. According to a previous study,[16] the first lithiation of FeS_2 proceeded *via* an intermediate Li_2FeS_2 by following a two-step reduction mechanism:

$$FeS_2 + 2Li^+ + 2e^- \rightarrow Li_2FeS_2 \quad (1)$$

$$Li_2FeS_2 + 2Li^+ + 2e^- \rightarrow 2Li_2S + Fe \quad (2)$$

After the first lithiation, very small Fe particles and Li_2S were generated in the final reduction products, which have been found by ^{57}Fe Mössbauer study[17,18] and suggested by density functional theory (DFT) simulation.[19] Upon the first delithiation, the scenario is more complicated, and instead of the starting material cubic-FeS_2, elemental sulfur, nonstoichiometric pyrrhotite-FeS_y, and orthorhombic-FeS_2 (marcasite) were produced according to the following reactions:[12,16]

$$2Li_2S + Fe \rightarrow Li_2FeS_2 + 2Li^+ + 2e^- \quad (3)$$

$$Li_2FeS_2 \rightarrow Li_{2-x}FeS_2 + xLi^+ + xe^- \quad (0 \le x \le 0.8) \quad (4)$$

$$Li_{2-x}FeS_2 \rightarrow 0.8\ \text{orthorhombic} - FeS_2 + 0.2FeS_{8/7} + 0.175S + (2-x)Li^+ + (2-x)e^- \quad (0.8 < x) \quad (5)$$

After the first delithiation, the Li−FeS_2 system is expected to become a hybrid of Li−iron sulfide cell and Li−sulfur cell. Upon cycling, a Li−FeS_2 battery will have to face the issues caused by the notorious long-chain lithium polysulfides, similar to those in Li−S batteries, such as side reactions with carbonate electrolyte, shuttle effect, loss of sulfur, and lithium metal corrosion.[11,14] Considering that Li−S chemistry has been intensively studied and some excellent approaches have been proposed to successfully mitigate the lithium polysulfides dissolution and reaction issues, we can draw lessons from the Li−S system to overcome the obstacles in the Li−FeS_2 system. For example, Lee's group has shown that by using solid electrolyte and ionic liquid electrolyte to suppress the lithium polysulfides solubility and reactivity with electrolyte,[2,12] an FeS_2 electrode demonstrated much more stable cycling performance than the same material tested in a conventional carbonate electrolyte. Recently, our group[20] and Chen *et al.*[21] simultaneously showed that, by simply replacing the carbonate electrolyte with an ether-based electrolyte, the cycling performance of FeS_2 in a sodium battery was substantially improved. These results clearly indicated the importance of electrolyte on the electrochemical performance of FeS_2 in rechargeable lithium/sodium batteries.

Besides lithium polysulfides dissolution and reaction, several other issues, such as volume change (~164.2% from FeS_2 to Fe and $2Li_2S$), sluggish reaction kinetics, and Fe^0 particle aggregation upon cycling,[11] could also cause severe capacity degradation. So far, a few nanostructured FeS_2 and FeS_2 composites (*e.g.*, high-purity FeS_2 nanowires,[4] FeS_2@C porous nano-octahedra,[5] FeS_2 embedded in stabilized polyacrylonitrile,[7] FeS_2 nanocrystals,[8] resilient carbon-encapsulated FeS_2,[10] *etc.*), some of which were prepared through quite cumbersome synthetic procedures, have been proposed to enhance the electrochemical performance of the Li−FeS_2 system by trying to solve the aforementioned issues. Although the reversibility of Li−FeS_2 has been improved, the reported cycling performance of Li−FeS_2 still showed unsatisfactory capacity retention, and the redox reaction mechanisms of the Li−FeS_2 system still seem unclear.[11]

In the present study, a self-standing FeS_2@carbon fiber composite electrode was developed with FeS_2 nanoparticles either embedded in or attached to the carbon fibers. It was reported that metal current collectors can affect the lithiation−delithiation profiles and cycling stability of the Li−FeS_2 system.[22] Here, the self-standing FeS_2@carbon fiber electrode could not only improve the reaction kinetics through nanosized FeS_2 and conductive network but also avoid the influence of current collector and/or other components (*e.g.*, binder) on the redox mechanisms and cycling stability of Li−FeS_2. The electrochemical performance of the FeS_2@carbon fiber electrode was tested under two different voltage ranges in two types of electrolyte, conventional carbonate electrolyte and a "solvent-in-salt"-type Li−S battery electrolyte.[23] It was found that by controlling the testing voltage in the range of 1.5−3.0 V (*vs* Li/Li^+) to limit the amount of inserted lithium, the reaction involving the production of Fe^0 and its associated volume changes was restrained so that the electrode could be stably cycled in the carbonate electrolyte, although the overall capacity

DOI: 10.1021/acsnano.5b07081
ACS Nano 2016, 10, 1529−1538

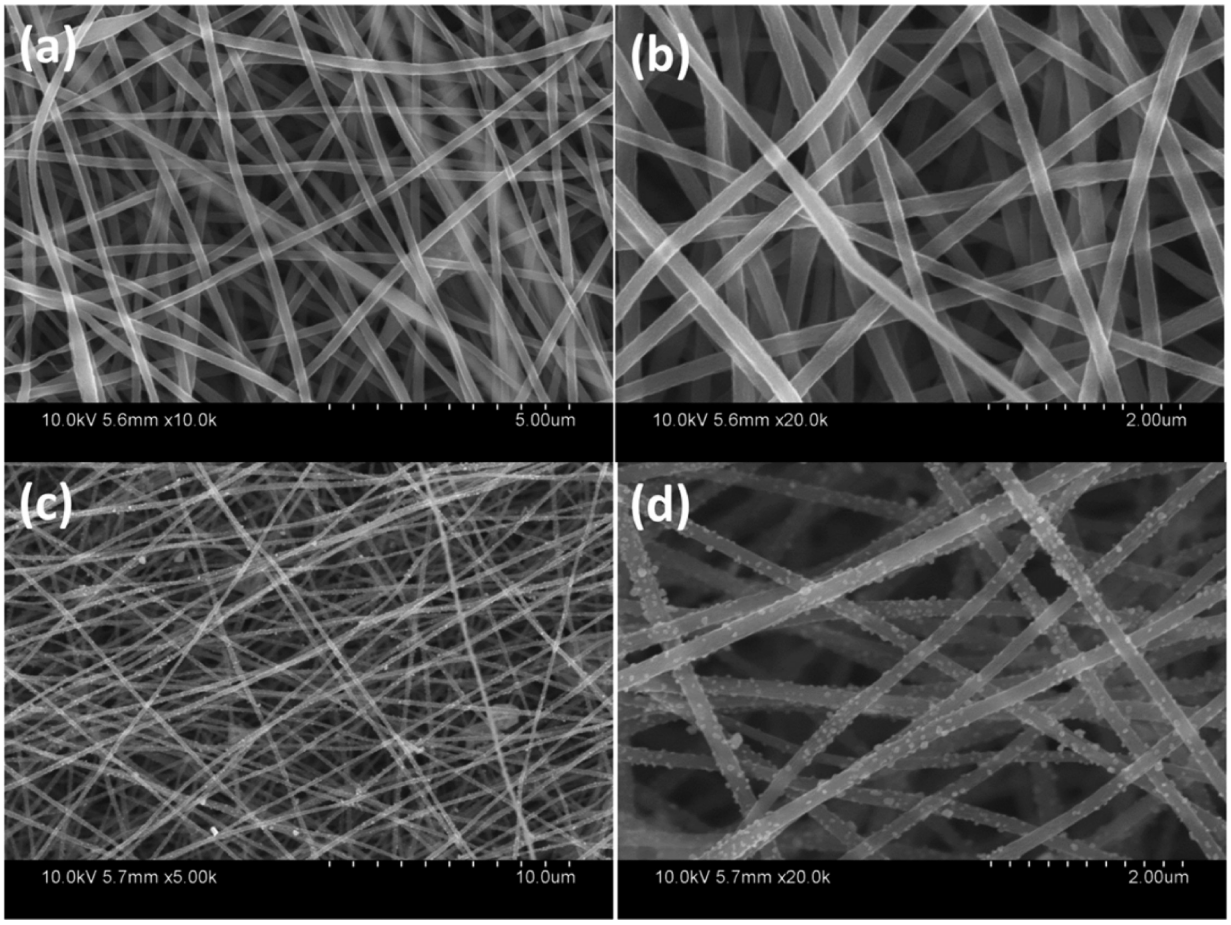

Figure 2. SEM images of carbonized PAN $Fe(C_5H_7O_3)_3$ fibers before (a,b) and after (c,d) sulfidation.

was low. Switching from the carbonate electrolyte to the solvent-in-salt-type Li−S battery electrolyte, the overall capacity of the electrode demonstrated a 3-fold increase, which was attributed to the suppressed lithium polysulfides dissolution and reaction. In the solvent-in-salt-type electrolyte, we observed that the Li−FeS_2 cell completely became a hybrid of the Li−sulfur and Li−iron sulfide systems after the initial few cycles, and the FeS_2@carbon fiber electrode was stably cycled in the voltage range of 1.5−3.0 V (*vs* Li/Li^+). To enhance the cycling stability of Li−FeS_2 in the voltage range of 1.0−3.0 V (*vs* Li/Li^+) and thus obtain more reversible lithium storage capacities, a thin layer of Al_2O_3 was coated onto the FeS_2@carbon fiber electrode by using atomic layer deposition (ALD). The Al_2O_3-coated electrode exhibited much more stable cycling behavior than the uncoated electrode in the voltage range of 1.0−3.0 V (*vs* Li/Li^+) and was able to provide a discharge energy density as high as 1300 Wh/kg-FeS_2 with a retention of 1100 Wh/kg-FeS_2 after 100 cycles, much higher than the theoretical energy density of the $LiCoO_2$ cathode (~550 Wh/kg-$LiCoO_2$). *Ex situ* scanning electron microscopy (SEM) results revealed that the ALD Al_2O_3 coating provided mechanical protection against the loss of contact between FeS_2 and current collector (~carbon fibers in the present study) and preserved the integrity of the electrodes.

RESULTS AND DISCUSSION

The FeS_2@carbon fiber electrode was prepared through electrospinning followed by vacuum sulfidation (see the Methods section for more details). Figure 1a shows the X-ray diffraction (XRD) pattern of the as-obtained FeS_2@carbon fiber electrode. All peaks can be assigned to cubic-FeS_2 (JCPDS no. 65-3321) without any detectable crystalline impurity. Figure 1b presents the thermogravimetric analysis (TGA) results for commercial FeS_2 from Sigma-Aldrich and FeS_2@carbon fiber electrode, tested in an air atmosphere. As shown in Figure 1b, under thermal oxidation, commercial FeS_2 started to lose weight at 450 °C and presented a final weight loss of 32.87% at 900 °C, very close to the theoretical weight loss (~33.33%) from FeS_2 to $0.5Fe_2O_3$ and manifesting that the oxidation product of FeS_2 was Fe_2O_3. The TGA result of FeS_2@carbon fiber electrode exhibited a slight weight loss (~5%) around 150 °C and a large weight loss around 350 °C. The first weight loss should be attributed to vaporization of absorbed water and oxidation of the uncarbonized chemical groups of polyacrylonitrile (PAN).[24] The second one was due to oxidation of carbon and FeS_2. Based on the weight percentage of the residue and the fact that FeS_2 was oxidized into Fe_2O_3, it can be calculated that the weight content of FeS_2 in the FeS_2@carbon fiber electrode was around 76.03%.

Figure 2 shows the SEM images of carbonized PAN $Fe(C_5H_7O_3)_3$ fibers before and after sulfidation. Before sulfidation (Figure 2a,b), the carbonized fibers presented a uniform diameter around 300 nm with a smooth surface, indicating that all Fe_2O_3 particles were encapsulated into the fibers, consistent with the transmission electron microscopy (TEM) images (Figure S1). After sulfidation (Figure 2c,d), the size of the fibers did not show noticeable change. However, small particles, which later were identified to be FeS_2 by TEM

DOI: 10.1021/acsnano.5b07081
ACS Nano 2016, 10, 1529−1538

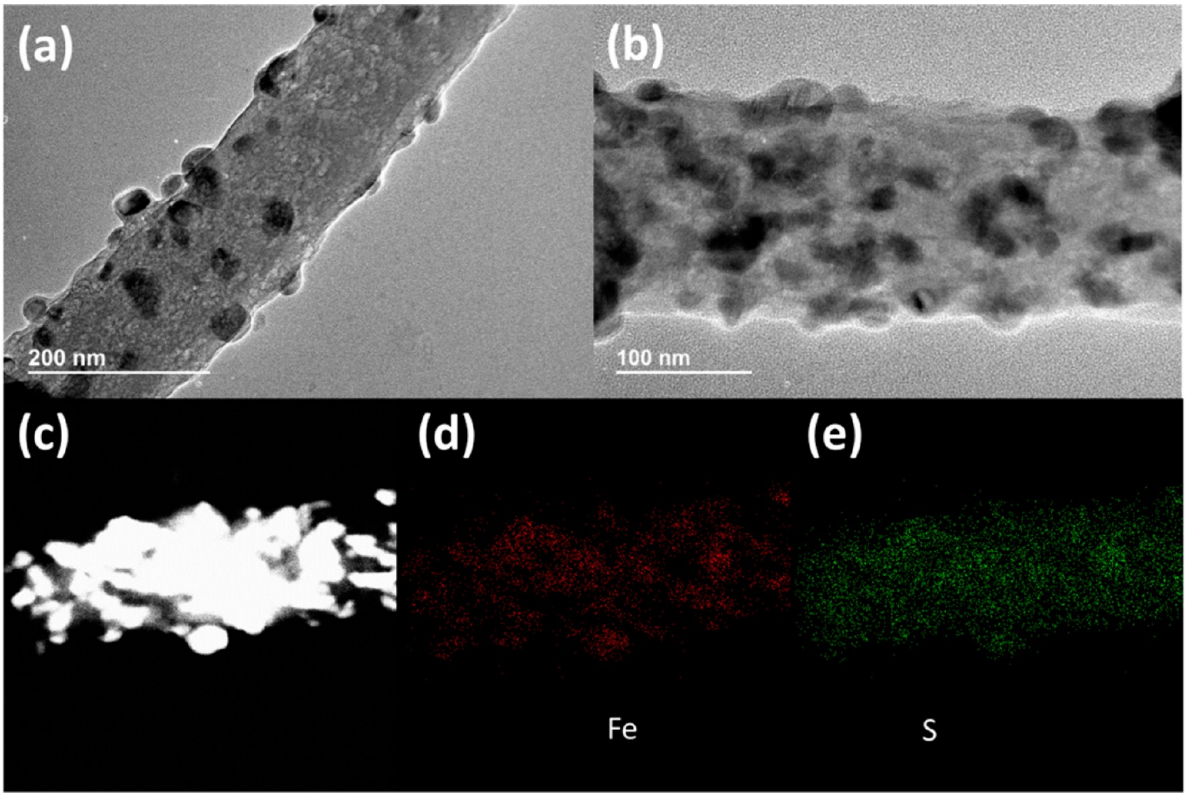

Figure 3. (a–c) TEM images and EDS elemental mapping for (d) iron and (e) sulfur for the FeS_2@carbon fiber shown in (c).

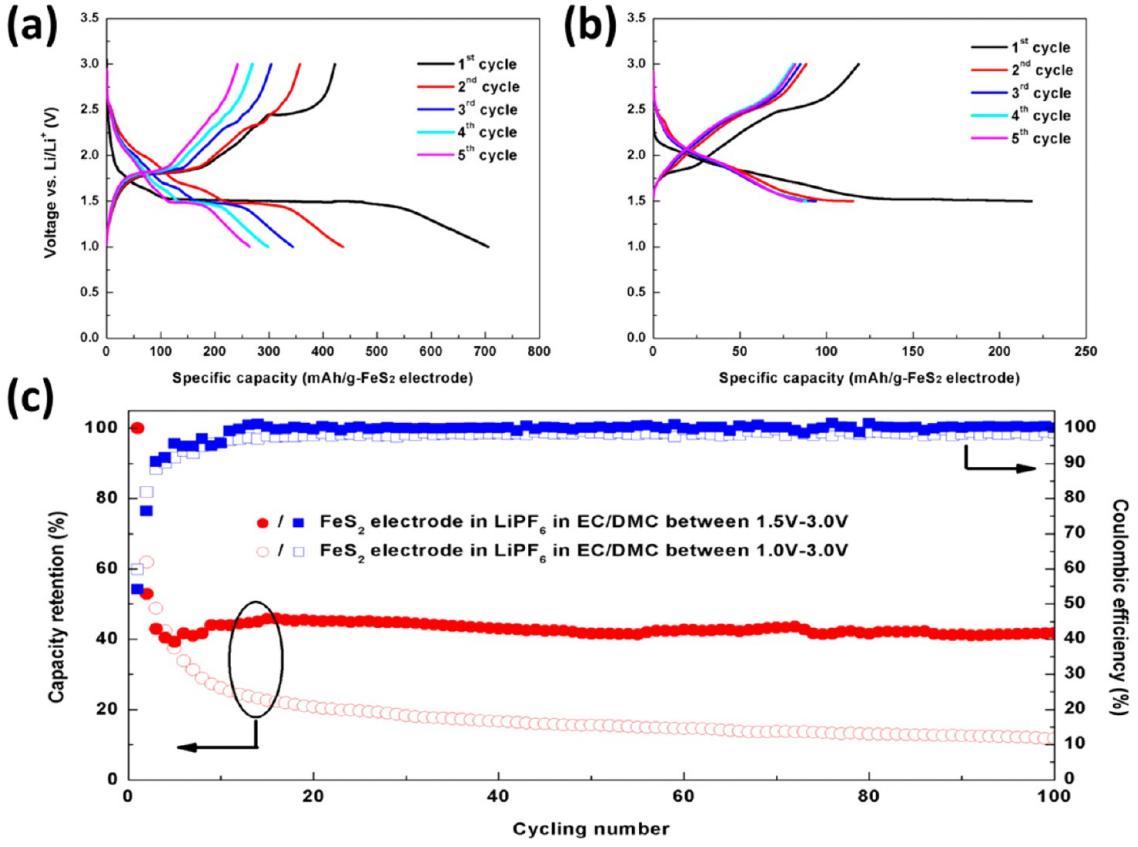

Figure 4. Electrochemical performance of FeS_2@carbon fiber electrode tested in carbonate electrolyte. Voltage profiles of the initial five cycles tested in the voltage range of (a) 1.0–3.0 V (*vs* Li/Li^+) and (b) 1.5–3.0 V (*vs* Li/Li^+) at 20 mA/g. (c) Cycling stability tests in the two different voltage ranges at 20 mA/g.

DOI: 10.1021/acsnano.5b07081
ACS Nano 2016, 10, 1529–1538

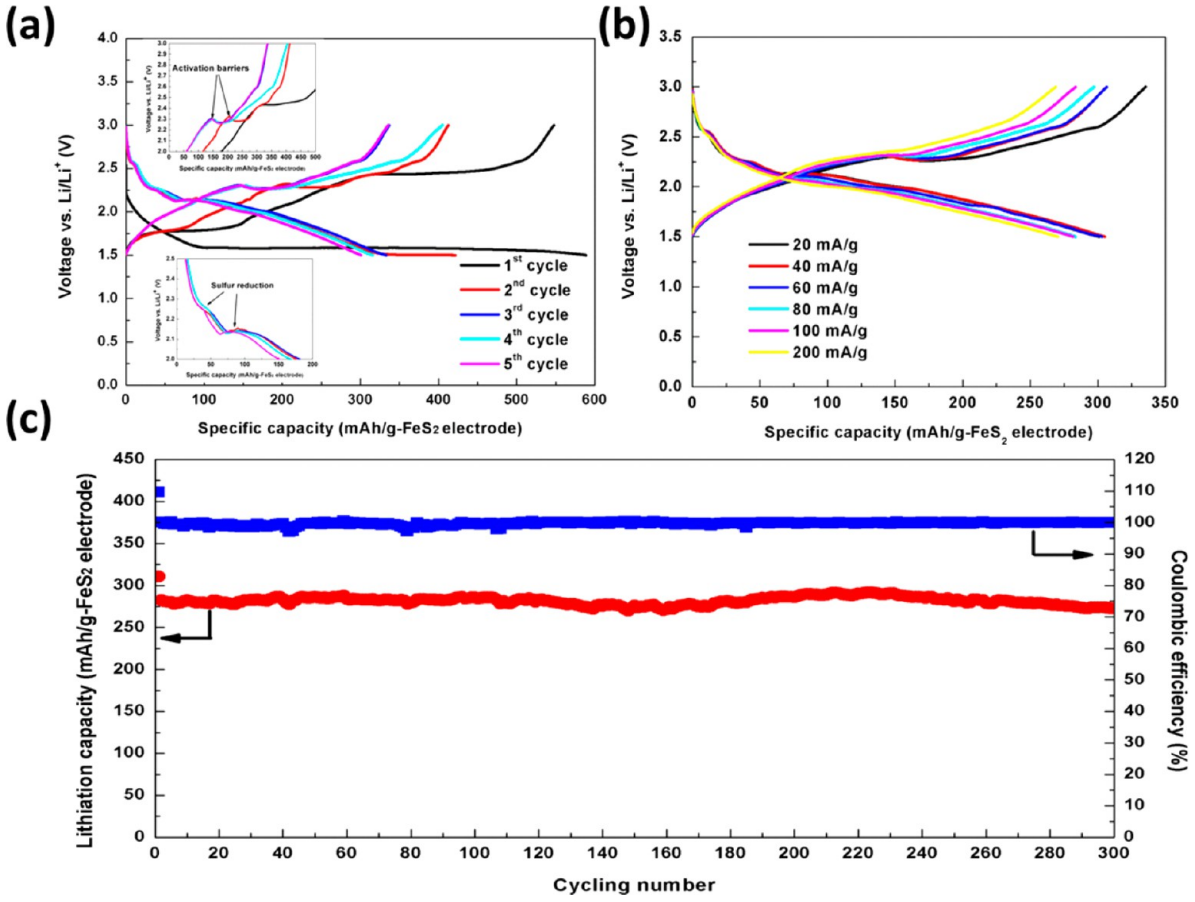

Figure 5. Electrochemical performance of the FeS_2@carbon fiber electrode tested in the solvent-in-salt-type electrolyte in the voltage range of 1.5−3.0 V (*vs* Li/Li^+). (a) Voltage profiles of the initial five cycles tested under 20 mA/g. (b) Voltage profiles under different current densities. (c) Cycling stability test under 200 mA/g (note: the electrode was precycled under 20 mA/g for five cycles).

energy-dispersive X-ray spectroscopy (EDS) elemental mapping (Figure 3d,e), emerged on the surface of the fibers (Figure 2c,d). This might be due to the aggregation of FeS_2 during the sulfidation process and the ∼160% volume expansion when Fe_2O_3 was transformed into $2FeS_2$ so that some Fe_2O_3 particles increased their size and broke the carbon fiber to appear on the surface. The increased size after the transition from Fe_2O_3 to $2FeS_2$ was also observed in our previous work.[20] Figure 3 shows the TEM images and EDS elemental mapping of FeS_2@carbon fiber electrode. Nanoparticles with diameters ranging from 20 to 50 nm were either encapsulated in or attached to the carbon fiber randomly (Figure 3a,b). The TEM EDS elemental mapping (Figure 3d,e) demonstrated that the nanoparticles were composed of iron and sulfur elements, manifesting that the nanoparticles were FeS_2 and agreeing with the XRD pattern.

Figure 4 shows the electrochemical performance of the FeS_2@carbon fiber electrode tested in carbonate electrolyte (1 M $LiPF_6$ in EC/DMC (ethylene carbonate/dimethyl carbonate) 1:1 by volume) under different voltage ranges. In Figure 4a, when the discharge−charge voltage range was selected to be 1.0−3.0 V (*vs* Li/Li^+), the first lithiation profile consisted of a sloped curve followed by a voltage plateau around 1.5 V and another sloped line to 1.0 V. We noticed that the first lithiation profile presented here was different with the one reported in previous work,[2,4,5,7,25] where mostly a sudden voltage drop was generally observed before the 1.5 V voltage plateau was touched. Thermodynamically, there should be two voltage regions during the first lithiation corresponding to reactions 1 and 2, as shown by Lee *et al.* through coulometric titration.[12] However, because of the slow reaction kinetics caused by the low diffusivity of the Li-ion into cubic-FeS_2, reactions 1 and 2 usually took place simultaneously around 1.5 V during the constant current discharge−charge, which has been observed by published work.[2,4,5,7,25] The observed difference for the initial lithiation profile between the present work and previous ones might be attributed to the small current density used here (20 mA/g-FeS_2 electrode) and the improved kinetics by nanosized FeS_2 particles and the unique one-dimensional carbon network of FeS_2@carbon fiber electrode. Compared with the first lithiation, subsequent lithiation profiles were different, which has been attributed to the different reaction kinetics and pathways between the first lithiation and the following ones.[12] The first delithiation curve contained two voltage plateaus. The lower plateau around 1.7 V was due to reaction 3, and the upper plateau around 2.4 V could be ascribed to reaction 5,[16] which vanished after the first delithiation, indicating the instability of reaction 5. Upon continuous cycling between 1.0 and 3.0 V, the voltage plateaus during lithiation (∼1.5 V due to reaction 2) and delithiation (∼1.7 V due to reaction 3) were gradually lost, resulting into the capacity decay.

Figure 4b shows the discharge−charge curves when the cell was cycled in the range of 1.5−3.0 V (*vs* Li/Li^+). Different from the gradually fading voltage plateaus in Figure 4a, the lithiation voltage plateau around 1.5 V and delithiation voltage plateau around 1.7 V quickly disappeared after the second cycle,

DOI: 10.1021/acsnano.5b07081
ACS Nano 2016, 10, 1529−1538

indicating that reactions 2 and 3 were suppressed in this voltage range. Figure 4c shows the capacity retention of the FeS_2@carbon fiber electrode tested in carbonate electrolyte under different voltage ranges. Although the absolute lithiation capacity was undoubtedly higher when the cell was discharged to 1.0 V, the capacity retention was much poorer compared with the cell discharged to 1.5 V. Also, the Coulombic efficiency was higher when 1.5 V was used as the cutoff voltage. In Figure 4, by simply choosing a cutoff voltage of 1.5 V to control the amount of inserted lithium ions, reactions 2 and 3 were restrained, as evidenced by the disappearance of voltage plateaus in Figure 4b after the initial cycle, and the volume change caused by reactions 2 and 3 should also be alleviated. As a consequence, after the second cycle, the capacity remained almost unchanged for the cell tested between 1.5 and 3.0 V. However, the absolute capacity of the electrode was only 100 mAh/g-electrode (~131 mAh/g-FeS_2), which was lower compared with intercalation-type cathodes.

Considering that sulfur will be generated after full delithiation by following reaction 5, the low capacity of the FeS_2@carbon fiber electrode in Figure 4b could be caused by the instability of Li−S chemistry in the carbonate electrolyte. To further enhance the capacity of the FeS_2@carbon fiber electrode, the electrode was tested in a previously proposed solvent-in-salt-type Li−S battery electrolyte (7 M LiTFSI in DOL/DME (1,3-dioxolane/dimethoxyethane) 1:1 by volume) (Figure 5). The solvent-in-salt-type Li−S battery electrolyte improved the electrochemical performance of Li−S chemistry by suppressing lithium dendrite growth and inhibiting lithium polysulfides dissolution.[23] As shown in Figure 5a, the first lithiation−delithiation profile was quite similar to the result shown in Figure 4b, except both the capacity and first cycle Coulombic efficiency were much higher in Figure 5a. However, the second lithiation curve was different from the one in Figure 4b, and it was composed of a short voltage plateau around 2.1 V followed by a sloped voltage profile and another voltage plateau around 1.5 V in the end. During the second delithiation, the 1.7 V voltage plateau shortened, and the 2.4 V plateau disappeared, indicating that the disproportionation reaction 5 did not take place during the second delithiation. Instead, the often observed activation process in Li−S batteries emerged (top inset in Figure 5a), which was due to the slow kinetics of oxidation from insoluble and insulating Li_2S to long-chain lithium polysulfides.[14] After the second delithiation, since the lithiation voltage plateau around 1.5 V ascribed to reaction 2 vanished, correspondingly, the delithiation voltage plateau around 1.7 V due to reaction 3 was completely absent.

Starting from the third cycle, the lithiation voltage plateau at 1.5 V vanished, but the short lithiation voltage plateau around 2.1 V and the following sloped voltage profile remained almost unchanged (Figure 5a). The lithiation capacity remained around 300 mAh/g-electrode. Considering that the FeS_2 content in the FeS_2@carbon fiber electrode was 76.03% and the negligible lithium storage capacity provided by carbon fibers in the voltage range of 1.5−3.0 V (*vs* Li/Li^+), this capacity corresponded to 395 mAh/g-FeS_2 and indicated that less than two lithium ions were inserted into FeS_2 (the theoretical capacity of FeS_2 is 894 mAh/g). Previous *in situ* Fe K-edge EXAFS and XANES analyses[26] and DFT calculations have suggested that if the inserted lithium was limited to two lithium ions, only $(S-S)^{2-}$ in FeS_2 will be reduced and oxidized.[12] Thus, we believe that reactions involving iron oxidation/reduction did not occur in the third and subsequent lithiation in Figure 5a, as evidenced by the disappearance of voltage plateaus corresponding to reactions 2 and 3. During the third and subsequent delithiation processes, before the voltage reached the Li_2S activation barrier, a sloped voltage profile with a capacity around 150 mAh/g-electrode was observed. We are aware that such a curve has never been reported for Li−S batteries. During the delithiation of the Li−S battery, the voltage usually quickly jumped to overcome the activation barrier with almost no capacity recorded prior to the activation voltage.[14] Based on the charge−discharge behavior of Li−Li_2FeS_2 cell and *in situ* XRD results, Fong *et al.*[16] have suggested that the Li−FeS_2 cell should present intercalation-type reversible reactions in the voltage region of 1.45−2.45 V (*vs* Li/Li^+) with a reversible capacity around 180 mAh/g-FeS_2. So we infer that this sloped voltage profile cannot be attributed to the oxidation of Li_2S but ought to originate from the delithiation of lithiated iron sulfide compounds. Based on the analysis of delithiation curves, the short lithiation voltage plateau around 2.1 V should originate from the reduction of long-chain lithium polysulfides to Li_2S, and the sloped voltage profile can be ascribed to lithiation of iron sulfide compounds.

In Figure 5a, the absence of the 2.1 V lithiation plateau during the first lithiation can rule out the possibility that the observed lithium−sulfur reaction was due to unwashed sulfur. Therefore, it can be safely concluded that the lithium−sulfur reaction was rooted in the electrochemically generated sulfur, which was initially produced by the disproportionation reaction of $Li_{2-x}FeS_2$ in the first cycle.[2,12,16] As presented in Figure 5a (bottom inset in Figure 5a), the length of the lithiation plateau was almost unchanged from the second to the fifth cycle, manifesting that the capacity provided by Li−S chemistry was constant in the solvent-in-salt electrolyte when the cell was cycled between 1.5 and 3.0 V. Assuming that sulfur can deliver its theoretical capacity (~1672 mAh/g-S) and based on the capacity (~100 mAh/g-electrode) above the discharge plateau around 2.1 V, it can be roughly estimated from eq 6 below that for 1 mol of FeS_2, approximately at least 0.29 mol of elemental sulfur should be produced in Figure 5a. This value is higher than the one (~0.175) shown in reaction 5, which was estimated from microsized FeS_2 in a solid-state cell by Lee *et al.*[12] The discrepancy might be caused by the different reaction kinetics between the present study and the previous one.

$$\frac{n_S}{n_{FeS_2}} = \frac{120\frac{g}{mol} \times \frac{100}{0.7603}\frac{mAh}{g}}{32\frac{g}{mol} \times 1672\frac{mAh}{g}} = 0.29 \quad (6)$$

The rate performance of the FeS_2@carbon fiber electrode in the solvent-in-salt electrolyte is shown in Figure 5b. Before the rate capability test, the cell was cycled under 20 mA/g for five cycles. As shown in Figure 5b, the FeS_2@carbon fiber electrode can provide an overall lithiation capacity of 300 mAh/g-electrode (~395 mAh/g-FeS_2) at 20 mA/g. This capacity is 3 times higher than that obtained in the carbonate electrolyte (~100 mAh/g-electrode in Figure 4b) in the same voltage range, which should be attributed to the stabilized Li−S chemistry by the solvent-in-salt electrolyte. When the current density was increased to 200 mA/g, the electrode can still present an overall lithiation capacity of 275 mAh/g-electrode (~362 mAh/g-FeS_2), higher than that of intercalation-type cathodes. Compared with the lithiation−delithiation curves at 20 mA/g, the voltage profiles at 200 mA/g only presented slightly increased polarization, implying the fast reaction

DOI: 10.1021/acsnano.5b07081
ACS Nano 2016, 10, 1529−1538

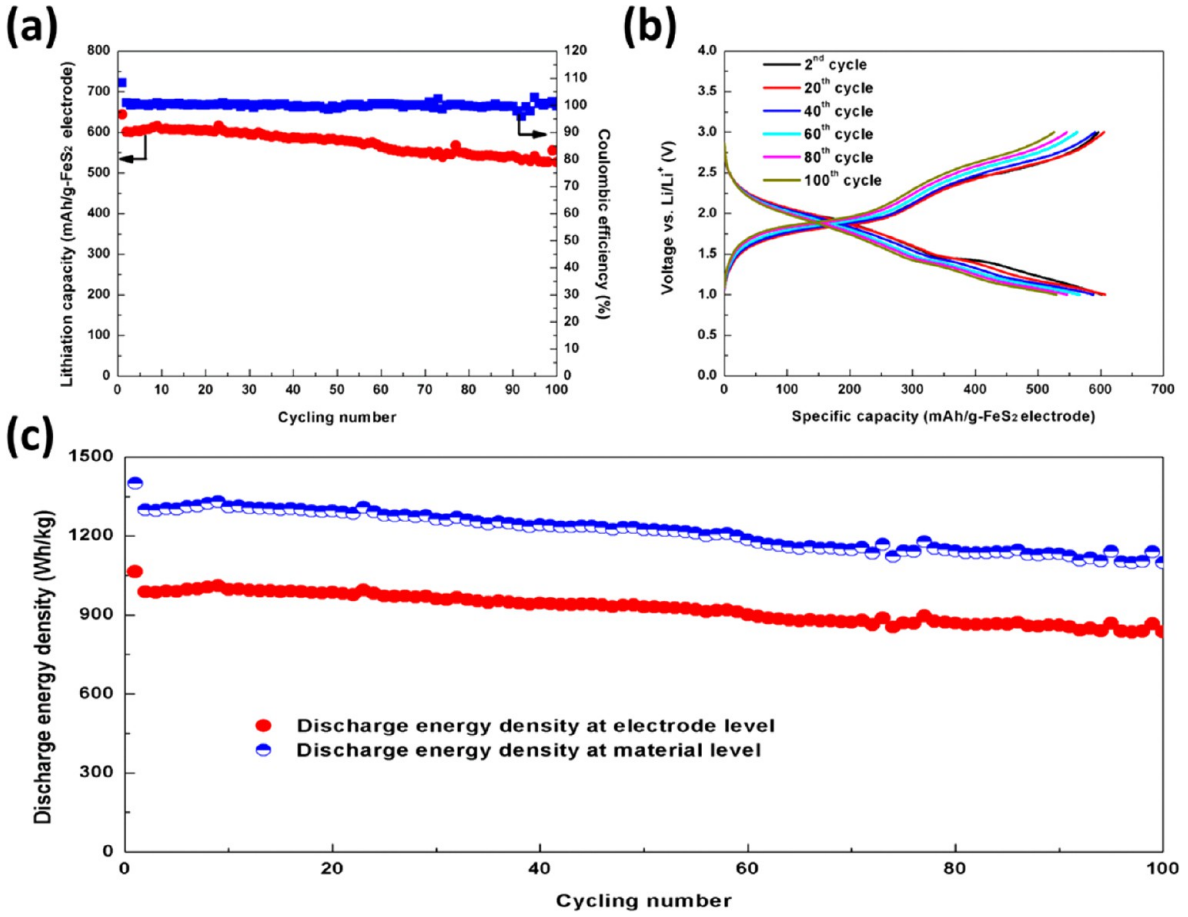

Figure 6. Electrochemical performance for the Al_2O_3-coated FeS_2@carbon fiber electrode tested in the solvent-in-salt electrolyte in the voltage range of 1.0−3.0 V (*vs* Li/Li^+). (a) Capacity retention test. (b) Lithiation−delithiation curves at different cycles. (c) Discharge energy density *vs* cycling number at the material level (~Wh/kg-FeS_2) and the electrode level (~Wh/kg-FeS_2 electrode).

kinetics of the FeS_2@carbon fiber electrode with the unique structure. Figure 5c shows the cycling performance of the FeS_2@carbon fiber electrode tested under 200 mA/g in the solvent-in-salt electrolyte. As shown in Figure 5c, the FeS_2@carbon fiber electrode presented stable cycling performance with almost no capacity decay over 300 cycles, and the Coulombic efficiency, defined by lithiation capacity divided by delithiation capacity, was close to 100% all the time. For comparison, the FeS_2@carbon fiber electrode was also tested in the solvent-in-salt electrolyte in the voltage range of 1.0−3.0 V (*vs* Li/Li^+) at 200 mA/g (Figure S2). As shown in Figure S2a, although the initial lithiation capacity was 550 mAh/g-electrode when the cell was discharged to 1.0 V, the capacity dropped to be below 275 mAh/g-electrode in 30 cycles with only 150 mAh/g-electrode remaining at the 60th cycle. Comparison between Figure 5c and Figure S2a indicated that the limited voltage range restrained the amount of inserted lithium to mitigate the associated detrimental effects on the cycling performance.

In Figure 5, after the electrochemical performance became stable, less than one-half of the theoretical capacity for FeS_2 was achieved, which seemed to be against the original intention of using FeS_2 as the cathode material, mainly due to its high theoretical capacity. To further increase the reversible capacity of FeS_2, attempts should be focused on stabilizing the low voltage region below 1.5 V. To unveil the mechanisms for the capacity decay, we checked the morphology of one after-cycled electrode, which was cycled in the voltage range of 1.0−3.0 V (*vs* Li/Li^+) in the solvent-in-salt-type electrolyte. As shown in Figure S3, *post mortem* SEM results of the after-cycled FeS_2@carbon fiber electrode clearly revealed that the surface of the carbon fibers became rough, and in comparison with the pristine electrode, no FeS_2 particles were found on the surface of the fibers, indicating the detachment of FeS_2 particles from the carbon fibers, probably caused by the repeated volume changes of FeS_2 during lithiation−delithiation. For electrode materials undergoing large volume fluctuations, the detachment between active materials and current collector was considered as one of the major reasons accounting for the capacity decay. Since carbon fibers were served as the current collector in the present study, the capacity degradation in Figure S2a should be mainly ascribed to the loss of electrical contact between FeS_2 and carbon fibers.

To improve the cycling stability of the FeS_2@carbon fiber electrodes in the voltage range of 1.0−3.0 V (*vs* Li/Li^+), we coated the whole electrode with a thin layer of Al_2O_3 (~5 nm) by using ALD. As demonstrated by previous works, Al_2O_3 coating, especially on the whole electrode, could greatly enhance the cycling performance of electrode materials (for example, Si,[27] MoO_3,[28,29] Sn[30]), which experienced large volume changes during electrochemical cycling, by increasing the adhesion of electrode materials on current collector and alleviating the mechanical degradation of electrodes.[29] Figure S4 shows the SEM EDS elemental mapping for the Al_2O_3-

DOI: 10.1021/acsnano.5b07081
ACS Nano 2016, 10, 1529−1538

coated FeS_2@carbon electrode. To get a better signal contrast, we intentionally chose only one fiber to do the mapping. As demonstrated in Figure S4, Al_2O_3 was successfully coated onto the FeS_2@carbon fiber.

The cycling performance of the Al_2O_3-coated FeS_2@carbon fiber electrode was tested under the voltage range of 1.0−3.0 V (*vs* Li/Li^+) in the solvent-in-salt electrolyte at 200 mA/g-electrode. As presented in Figure 6a, the Al_2O_3-coated electrode exhibited much better cycling performance than the uncoated one. The lithiation capacity of the Al_2O_3-coated electrode was 600 mAh/g-electrode in the second cycle and remained at 530 mAh/g-electrode in the 100 cycles with a capacity decay rate of 0.12% per cycle. The lithiation−delithiation curves maintained similar shapes upon cycling, with gradually increased polarization (Figure 6b), which was less than 120 mV from the second cycle to the 100th cycle, much smaller compared to the uncoated electrode (Figure S2b) tested in the same voltage range. The discharge energy density of the Al_2O_3-coated FeS_2@carbon fiber electrode initially reached 1000 Wh/kg-electrode (~1300 Wh/kg-FeS_2 at material level) with a retention of 840 Wh/kg-electrode (~1110 Wh/kg-FeS_2) after 100 cycles (Figure 6c), much higher than other reported studies for FeS_2.[2,4−7]

Figure 7 schematically illustrated the mechanisms for the enhanced cycling stability by Al_2O_3 coating in the voltage range

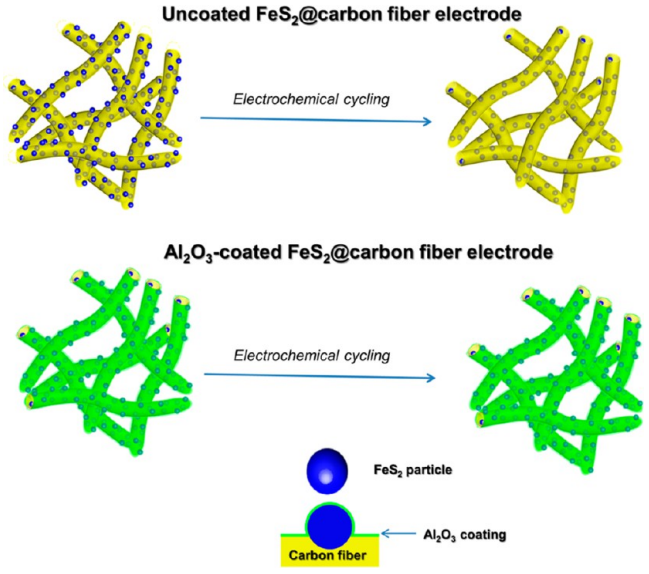

Figure 7. Schematic illustration of mechanisms for the enhanced cycling stability by Al_2O_3 coating in the voltage range of 1.0−3.0 V (*vs* Li/Li^+).

of 1.0−3.0 V (*vs* Li/Li^+). For the uncoated FeS_2@carbon fiber electrode, repeated volume changes will cause FeS_2 particles to fall off carbon fibers, leading to the capacity decay. For the Al_2O_3-coated electrodes, the Al_2O_3 coating plays a three-fold role. First, it could improve the integrity of electrodes. After 100 charge−discharge cycles, the morphology of the Al_2O_3-coated electrode was examined by SEM. In sharp contrast with the uncoated electrode, we observed that FeS_2 particles were still well anchored on the carbon fibers (Figure S5), which should be attributed to the mechanical protection provided by the conformal Al_2O_3 coating. Second, the Al_2O_3 coating could serve as an artificial barrier to restrain the lithium polysulfides dissolution and mitigate the shuttle effects as it has been used to enhance the electrochemical performance of Li−S chemistry.[31,32] Third, upon electrochemical cycling, AlF_3 and $LiAlO_2$ would be formed on the top of Al_2O_3 coating layer due to the interactions between electrolyte salt (~LiTFSI) and Al_2O_3 as confirmed by synchrotron-based XPS results;[31] AlF_3 was able to enhance the Li-ion ionic conductivity, and $LiAlO_2$ could decrease the energy barrier for lithiation, both of which can facilitate the kinetics of Li-ion insertion.[27,31]

CONCLUSION

In summary, we have developed a self-standing FeS_2@carbon fiber electrode with FeS_2 nanoparticles either encapsulated in or attached to the interconnected one-dimensional carbon fibers. The FeS_2@carbon fiber electrode was tested under different voltage ranges (1.0−3.0 and 1.5−3.0 V *vs* Li/Li^+) in two types of electrolyte, 1 M $LiPF_6$ in EC/DMC 1:1 by volume and 7 M LiTFSI in DOL/DME 1:1 by volume. The electrochemical tests in the carbonate electrolyte (1 M $LiPF_6$ in 1:1 EC/DMC) indicated that by limiting the testing voltage range to 1.5−3.0 V (*vs* Li/Li^+) to restrain the amount of inserted lithium, the FeS_2@carbon fiber electrode could be stably cycled in carbonate electrolyte, although the overall capacity was only around 100 mAh/g-electrode. Switching from the carbonate electrolyte to the solvent-in-salt-type Li−S battery electrolyte (7 M LiTFSI in DOL/DME 1:1 by volume), the overall lithiation capacity of the FeS_2@carbon fiber electrode was increased to 300 mAh/g-electrode. By analyzing the lithiation−delithiation profiles, we observed that the Li−FeS_2 system transformed into a hybrid of a Li−sulfur system and a Li−iron sulfide system. Thus, the enhanced capacity in the solvent-in-salt electrolyte compared with the carbonate electrolyte can be ascribed to the stabilized Li−S chemistry by the solvent-in-salt electrolyte. Exceptional cycling stability was obtained when the FeS_2@carbon fiber electrode was tested in the solvent-in-salt electrolyte in the voltage range of 1.5−3.0 V (*vs* Li/Li^+); the electrode presented an overall capacity of 275 mAh/g-electrode with almost no capacity decay observed during 300 lithiation−delithiation cycles at 200 mA/g-electrode. By contrast, the electrochemical performance of the bare FeS_2@carbon fiber electrode was very poor in the voltage range of 1.0−3.0 V (*vs* Li/Li^+). By further applying a thin layer (~5 nm) of Al_2O_3 coating on the whole FeS_2@carbon fiber electrodes to prevent the mechanical degradation, the electrode demonstrated great electrochemical performance in the voltage range of 1.0−3.0 V (*vs* Li/Li^+). In this voltage range, the FeS_2@carbon fiber electrode presented a lithiation capacity of 600 mAh/g-electrode with a discharge energy density initially reaching 1000 Wh/kg-electrode and was retained at 840 Wh/kg-electrode after 100 cycles. Considering its low cost, earth abundance, relative safety, and maturity in commercial primary batteries, it is expected that the rechargeable Li−FeS_2 system will become competitive with the Li−S system in the future.

METHODS

Synthesis of FeS_2@Carbon Fiber Electrode. All reagents were purchased from Sigma-Aldrich and used without further purification. To synthesize the FeS_2@carbon fiber electrode, the Fe_2O_3@carbon fiber composite was first prepared by electrospinning. Briefly, 1.413 g of iron(III) acetylacetonate ($Fe(C_5H_7O_3)_3$, 97%) was dissolved into 10 mL of *N*,*N*-dimethylformamide with a concentration of 0.4 M. Then, 0.7 g of PAN was added into the solution with vigorous stirring at 50 °C overnight. The obtained solution was electrospun into fibers. The solution feeding rate was set to be 3 mL/h; the distance between

DOI: 10.1021/acsnano.5b07081
ACS Nano 2016, 10, 1529−1538

the needle tip and rotating drum fiber collector was 15 cm, and a high voltage of 15 kV was used during the electrospinning process. The collected polymer fibers were first stabilized in air at 250 °C for 2 h with a heating rate of 10 °C/min, followed by a carbonization process in a tube furnace at 600 °C for 5 h under an argon atmosphere with a heating rate of 5 °C/min. After the carbonization process, a composite of Fe_2O_3@carbon fibers was obtained.[33] The obtained Fe_2O_3@carbon fibers were sealed with sulfur in a weight ratio of 1:2 in a glass tube under vacuum conditions, which was then heated to 600 °C and held for 6 h. After the glass tube naturally cooled to room temperature, the sample was collected and washed with carbon disulfide (CS_2) to remove the excess sulfur. Finally, the FeS_2@carbon fiber electrode was obtained by drying the CS_2-washed sample in a vacuum oven set at 100 °C overnight.

Atomic Layer Deposition. A layer of Al_2O_3 with 5 nm thickness was deposited onto the FeS_2@carbon fiber electrode by using an ALD system (Beneq TFS 500) with high-purity nitrogen at 150 °C as the carrier gas. For each ALD Al_2O_3 cycle, alternating flows of trimethylaluminum (4 s, Al precursor) and water (4 s, oxidant) separated by flows of pure nitrogen gas (4 and 10 s, respectively, carrier and cleaning gas) were applied. The thickness of the deposited Al_2O_3 layer was around 1 Å per pulse cycle. Thus, for a thickness of 5 nm, 50 cycles of ALD Al_2O_3 were used.

Material Characterizations. The crystal structure of the FeS_2@carbon fiber electrode was characterized by using powder X-ray diffraction on a D8 Advanced with LynEye and SolX (Bruker AXS, WI, USA) with a Cu Kα radiation source operated at 40 kV and 40 mA in the 2θ range of 20−70° at the X-ray Crystallographic Center at the University of Maryland. TGA was used to determine the percentage of carbon in the FeS_2@carbon fiber electrode. The sample was loaded into the TGA equipment (SDT Q600, TA Instruments) and heated from room temperature to 900 °C in an air atmosphere with a heating rate of 10 °C/min. The morphology of samples was characterized by Hitachi SU-70 analytical ultra-high-resolution SEM and JEOL 2100F field emission TEM at the NanoCenter at the University of Maryland. Before taking the SEM images for the after-cycled electrodes, the electrodes were taken out from coin cells, which were at the fully delithiated state. Then, the electrodes were immersed into propylene carbonate overnight and subsequently thoroughly rinsed with propylene carbonate to remove the salt residues. The TEM sample was prepared by dispersing the electrodes in ethanol through ultrasonication, and then the dispersion was dropped onto TEM grids.

Electrochemical Tests. The as-prepared FeS_2@carbon fiber electrodes were directly assembled into coin cells without using any binder or metal current collector. Two different types of electrolyte, namely, 1 M $LiPF_6$ in EC/DMC (ethylene carbonate/dimethyl carbonate) 1:1 by volume and 7 M LiTFSI in DOL/DME (1,3-dioxolane/dimethoxyethane) 1:1 by volume, were used for the coin cells preparation. Coin cells, consisting of a lithium foil counter electrode, an FeS_2@carbon fiber working electrode, Celgard 3501 microporous film separator, and one of above two electrolytes, were assembled in an argon-filled glovebox with both water and oxygen content <0.5 ppm. The loading weight of the FeS_2@carbon fiber electrode was around 2 mg/cm^2. For all coin cells, the electrolyte/FeS_2 ratio was around 1:50 L/g.

Constant current discharge−charge experiments were tested on an Arbin battery test station (BT2000, Arbin Instruments, USA). Coin cells were charged−discharged between different voltage ranges. After the cell reached the cutoff voltages, it was relaxed for 1 min before subsequent discharge or charge. For the cycling stability tests, coin cells were precycled under 20 mA/g for five cycles. Both capacities and charge−discharge current densities were calculated with respect to the total weight of the self-standing electrodes.

ASSOCIATED CONTENT

Supporting Information

The Supporting Information is available free of charge on the ACS Publications website at DOI: 10.1021/acsnano.5b07081.

TEM images of carbonized PAN $Fe(C_5H_7O_3)_3$ fiber, electrochemical performance of the FeS_2@carbon fiber electrode tested in solvent-in-salt electrolyte under 1.0−3.0 V, SEM images for the FeS_2@carbon fiber electrode after 60 lithiation−delithiation cycles in the solvent-in-salt-type electrolyte in the voltage range of 1.0−3.0 V, SEM image and EDS elemental mapping of the Al_2O_3-coated FeS_2@carbon fiber, and SEM images and EDS element mapping of the Al_2O_3-coated FeS_2@carbon fiber electrode after 100 lithiation−delithiation cycles are shown in Figures S1−S5 (PDF)

AUTHOR INFORMATION

Corresponding Author

*E-mail: cswang@umd.edu.

Notes

The authors declare no competing financial interest.

ACKNOWLEDGMENTS

The authors acknowledge the financial support of the Army Research Lab under Contract No. W911VF1420031, and the technical support from Maryland Nanocenter and its Nisplab. The authors also thank Prof. Micheal R. Zachariah and Dr. Wenbo Zhou for their kind help on the TGA test.

REFERENCES

(1) Poizot, P.; Laruelle, S.; Grugeon, S.; Dupont, L.; Tarascon, J.-M. Nano-Sized Transition-Metal Oxides as Negative-Electrode Materials for Lithium-Ion Batteries. *Nature* **2000**, *407*, 496−499.

(2) Evans, T.; Piper, D. M.; Kim, S. C.; Han, S. S.; Bhat, V.; Oh, K. H.; Lee, S.-H. Ionic Liquid Enabled FeS_2 for High-Energy-Density Lithium-Ion Batteries. *Adv. Mater.* **2014**, *26*, 7386−7392.

(3) Hu, Z.; Zhang, K.; Zhu, Z.; Tao, Z.; Chen, J. FeS_2 Microspheres with an Ether-Based Electrolyte for High-Performance Rechargeable Lithium Batteries. *J. Mater. Chem. A* **2015**, *3*, 12898−12904.

(4) Li, L.; Cabán-Acevedo, M.; Girard, S. N.; Jin, S. High-Purity Iron Pyrite (FeS_2) Nanowires as High-Capacity Nanostructured Cathodes for Lithium-Ion Batteries. *Nanoscale* **2014**, *6*, 2112−2118.

(5) Liu, J.; Wen, Y.; Wang, Y.; van Aken, P. A.; Maier, J.; Yu, Y. Carbon-Encapsulated Pyrite as Stable and Earth-Abundant High Energy Cathode Material for Rechargeable Lithium Batteries. *Adv. Mater.* **2014**, *26*, 6025−6030.

(6) Liu, L.; Yuan, Z.; Qiu, C.; Liu, J. A Novel FeS_2/CNT Micro-Spherical Cathode Material with Enhanced Electrochemical Characteristics for Lithium-Ion Batteries. *Solid State Ionics* **2013**, *241*, 25−29.

(7) Son, S.-B.; Yersak, T. A.; Piper, D. M.; Kim, S. C.; Kang, C. S.; Cho, J. S.; Suh, S.-S.; Kim, Y.-U.; Oh, K. H.; Lee, S.-H. A Stabilized PAN-FeS_2 Cathode with an EC/DEC Liquid Electrolyte. *Adv. Energy Mater.* **2014**, *4* (1−5), 1300961.

(8) Walter, M.; Zünd, T.; Kovalenko, M. V. Pyrite (FeS_2) Nanocrystals as Inexpensive High-Performance Lithium-Ion Cathode and Sodium-Ion Anode Materials. *Nanoscale* **2015**, *7*, 9158−9163.

(9) Wen, X.; Wei, X.; Yang, L.; Shen, P. K. Self-Assembled FeS_2 Cubes Anchored on Reduced Graphene Oxide as an Anode Material for Lithium Ion Batteries. *J. Mater. Chem. A* **2015**, *3*, 2090−2096.

(10) Yoder, T. S.; Tussing, M.; Cloud, J. E.; Yang, Y. Resilient Carbon Encapsulation of Iron Pyrite (FeS_2) Cathodes in Lithium Ion Batteries. *J. Power Sources* **2015**, *274*, 685−692.

(11) Zhang, S. S. The Redox Mechanism of FeS_2 in Non-Aqueous Electrolytes for Lithium and Sodium Batteries. *J. Mater. Chem. A* **2015**, *3*, 7689−7694.

(12) Yersak, T. A.; Macpherson, H. A.; Kim, S. C.; Le, V.-D.; Kang, C. S.; Son, S.-B.; Kim, Y.-H.; Trevey, J. E.; Oh, K. H.; Stoldt, C.; Lee, S.-H. Solid State Enabled Reversible Four Electron Storage. *Adv. Energy Mater.* **2013**, *3*, 120−127.

DOI: 10.1021/acsnano.5b07081
ACS Nano 2016, 10, 1529−1538

(13) Shao-Horn, Y.; Osmialowski, S.; Horn, Q. C. Nano-FeS_2 for Commercial Li/FeS_2 Primary Batteries. *J. Electrochem. Soc.* **2002**, *149*, A1499−A1502.
(14) Nazar, L. F.; Cuisinier, M.; Pang, Q. Lithium-Sulfur Batteries. *MRS Bull.* **2014**, *39*, 436−442.
(15) Ma, L.; Hendrickson, K. E.; Wei, S.; Archer, L. A. Nanomaterials: Science and Applications in the Lithium-Sulfur Battery. *Nano Today* **2015**, *10*, 315−338.
(16) Fong, R.; Dahn, J. R.; Jones, C. H. W. Electrochemistry of Pyrite-Based Cathodes for Ambient Temperature Lithium Batteries. *J. Electrochem. Soc.* **1989**, *136*, 3206−3210.
(17) Jones, C. H. W.; Kovacs, P. E.; Sharma, R. D.; McMillan, R. S. ^{57}Fe MÖssbauer Spectroscopy of Reduced Cathodes in the Li/FeS_2 Battery System: Evidence for Superparamagnetism. *J. Phys. Chem.* **1990**, *94*, 832−836.
(18) Jones, C. H. W.; Kovacs, P. E.; Sharma, R. D.; McMillan, R. S. An ^{57}Fe MÖssbauer Study of the Intermediates Formed in the Reduction of FeS_2 in the Li/FeS_2 Battery System. *J. Phys. Chem.* **1991**, *95*, 774−779.
(19) Yamaguchi, Y.; Takeuchi, T.; Sakaebe, H.; Kageyama, H.; Senoh, H.; Sakai, T.; Tatsumi, K. Ab Initio Simulations of Li/Pyrite-MS_2 (M = Fe, Ni) Battery Cells. *J. Electrochem. Soc.* **2010**, *157*, A630−A635.
(20) Zhu, Y.; Suo, L.; Gao, T.; Fan, X.; Han, F.; Wang, C. Ether-Based Electrolyte Enabled Na/FeS_2 Rechargeable Batteries. *Electrochem. Commun.* **2015**, *54*, 18−22.
(21) Hu, Z.; Zhu, Z.; Cheng, F.; Zhang, K.; Wang, J.; Chen, C.; Chen, J. Pyrite FeS_2 for High-Rate and Long-Life Rechargeable Sodium Batteries. *Energy Environ. Sci.* **2015**, *8*, 1309−1316.
(22) Wang, Y.; Liao, H.; Wang, J.; Qian, X.; Zhu, Y.; Cheng, S. Effects of Current Collectors on Electrochemical Performance of FeS_2 for Li-Ion Battery. *Int. J. Electrochem. Sci.* **2013**, *8*, 4002−4009.
(23) Suo, L.; Hu, Y.-S.; Li, H.; Armand, M.; Chen, L. A New Class of Solvent-in-Salt Electrolyte for High-Energy Rechargeable Metallic Lithium Batteries. *Nat. Commun.* **2013**, *4*, 1481.
(24) Cho, C. W.; Cho, D.; Ko, Y.-G.; Kwon, O. H.; Kang, I. Stabilization, Carbonization, and Characterization of PAN Precursor Webs Processed by Electrospinning Technique. *Carbon Lett.* **2007**, *8*, 313−320.
(25) Takeuchi, T.; Kageyama, H.; Nakanishi, K.; Inada, Y.; Katayama, M.; Ohta, T.; Senoh, H.; Sakaebe, H.; Sakai, T.; Tatsumi, K.; Kobayashi, H. Improvement of Cycle Capability of FeS_2 Positive Electrode by Forming Composites with Li_2S for Ambient Temperature Lithium Batteries. *J. Electrochem. Soc.* **2012**, *159*, A75−A84.
(26) Totir, D. A.; Bae, I. T.; Hu, Y.; Antonio, M. R.; Stan, M. A.; Scherson, D. A. *In Situ* Fe K-Edge X-Ray Absorption Fine Structure of a Pyrite Electrode in a Li/Polyethylene Oxide($LiClO_4$)/FeS_2 Battery Environment. *J. Phys. Chem. B* **1997**, *101*, 9751−9756.
(27) Xiao, X.; Lu, P.; Ahn, D. Ultrathin Multifunctional Oxide Coatings for Lithium Ion Batteries. *Adv. Mater.* **2011**, *23*, 3911−3915.
(28) Riley, L. A.; Cavanagh, A. S.; George, S. M.; Jung, Y. S.; Yan, Y.; Lee, S.-H.; Dillon, A. C. Conformal Surface Coatings to Enable High Volume Expansion Li-Ion Anode Materials. *ChemPhysChem* **2010**, *11*, 2124−2130.
(29) Riley, L. A.; Cavanagh, A. S.; George, S. M.; Lee, S.-H.; Dillon, A. C. Improved Mechanical Integrity of ALD-Coated Composite Electrodes for Li-Ion Batteries. *Electrochem. Solid-State Lett.* **2011**, *14*, A29−A31.
(30) Han, X.; Liu, Y.; Jia, Z.; Chen, Y.-C.; Wan, J.; Weadock, N.; Gaskell, K. J.; Li, T.; Hu, L. Atomic-Layer-Deposition Oxide Nanoglue for Sodium Ion Batteries. *Nano Lett.* **2014**, *14*, 139−147.
(31) Li, X.; Liu, J.; Wang, B.; Banis, M. N.; Xiao, B.; Li, R.; Sham, T.-K.; Sun, X. Nanoscale Stabilization of Li−Sulfur Batteries by Atomic Layer Deposited Al_2O_3. *RSC Adv.* **2014**, *4*, 27126−27129.
(32) Yu, M.; Yuan, W.; Li, C.; Hong, J.-D.; Shi, G. Performance Enhancement of a Graphene−Sulfur Composite as a Lithium−Sulfur Battery Electrode by Coating with an Ultrathin Al_2O_3 Film *via* Atomic Layer Deposition. *J. Mater. Chem. A* **2014**, *2*, 7360−7366.
(33) Zhang, X.; Liu, H.; Petnikota, S.; Ramakrishna, S.; Fan, H. J. Electrospun Fe_2O_3−Carbon Composite Nanofibers as Durable Anode Materials for Lithium Ion Batteries. *J. Mater. Chem. A* **2014**, *2*, 10835−10841.

DOI: 10.1021/acsnano.5b07081
ACS Nano 2016, 10, 1529−1538